

# TTM: Terrain Traversability Mapping for Autonomous Excavators

Tianrui Guan<sup>1\*</sup> Zhenpeng He<sup>1</sup> Dinesh Manocha<sup>2</sup> Liangjun Zhang<sup>1</sup>

<sup>1</sup> Robotics and Auto-Driving Laboratory, Baidu Research

<sup>2</sup> University of Maryland, College Park

## Abstract

We present *Terrain Traversability Mapping (TTM)*, a real-time mapping approach for terrain traversability estimation and path planning for autonomous excavator applications in an unstructured environment. We propose an efficient learning-based geometric method to extract terrain features from RGB images and 3D pointclouds and incorporate them into a global map for planning and navigation. Our method can adapt to changing environments and update the terrain information in real time. Moreover, we prepare a novel dataset, the *Complex Worksite Terrain (CWT)* dataset, which consists of RGB images from construction sites with seven categories based on navigability. We improve the previous SOTA methods by 4.17% to 30.48% in terms of accuracy and reduce MSE on the traversability map by 13.8% to 71.4%. We have combined our mapping approach with planning and control modules in an autonomous excavator navigation system and observe 49.3% improvement in the overall success rate. Based on TTM, we demonstrate the first autonomous excavator that can navigate through unstructured environments consisting of deep pits, steep hills, rock piles, and other complex terrain features.

## 1. Introduction

Excavators are one of the most common types of heavy-duty machinery used for earth-moving activities, including mining, construction, environmental restoration, etc. As the demand for excavators increases, many autonomous excavator systems [21, 40, 56] have been proposed for material loading tasks, which involve perception and motion planning techniques. Autonomous excavator system (AES) [56] is the first to perform loading tasks in real-world scenarios.

In this paper, we address some of the challenges related to perception and its impact on planning for autonomous excavation. In general, perception in unstructured environments such as excavation has many challenges. There have been many works related to unstructured environments, in-



Figure 1. We highlight our mapping algorithm, TTM, the operating environment, and the input and output of our approach. **Top left:** Sensors on the excavator, including RGB cameras and Livox LiDAR. **Top right:** Detection region from a third-person perspective. **Middle left:** Frontal view captured by the camera. **Middle right:** Semantic segmentation output, where green, yellow, and maroon correspond to flat region, bumpy region, and rock, respectively. **Bottom left:** Colored pointcloud with semantic labels. **Bottom right:** Terrain traversability output, where the traversability value decreases from green to grey.

cluding perception and terrain classification [13, 43, 48] and navigation [18, 23, 25, 33]. Applications in unstructured, hazardous environments have even more difficulties in terms of robustness and limitations on the computational budget. For example, we cannot assume access to large GPUs or clusters for excavators operating in hazardous environments.

Traversability is a term that encompasses both perception and navigation. It has been well-studied for decade, and there have been many works [6, 9, 27, 44, 57] on traversability estimation for planning and navigation. Terrain traversability is a binary value, or a probability score,

\*Work done during an internship at Baidu RAL.

measuring the difficulty of navigating a region through perception sensors like camera and LiDAR. Terrain traversability estimation is a critical step between perception and navigation. In many cases [14, 33], a method capable of detecting obstacles and distinguishing road and non-road regions is sufficient for navigation. On the other hand, in an unstructured, hazardous environment where off-road navigation is unavoidable, there are many factors that must be considered, including efficiency, adaptability, and safety. In such case, not only a more detailed classification according to terrain features is needed, but also a continuous value for traversability is preferred to describe the complication of terrain and provide the best option for the navigation module. Therefore, using a better algorithm to obtain a traversable region is an essential first step for reliable navigation in unstructured scene.

**Main Results:** We present Terrain Traversability Mapping (TTM), a real-time mapping approach for terrain traversability classification and navigation. We propose an efficient semantic-geometric fusion method to extract traversability maps for planning and navigation. Our method leverages the physical and computational constraints of the robot, including maximum climbing degree, width of the body, run-time, etc. The novel aspects of our work include:

1. We present a real-time terrain traversability estimation and mapping algorithm (TTM) from 3D LiDAR and RGB camera inputs for planning and navigation. We develop a novel learning-based geometric fusion solution considering machine specifications and hardware limitation for terrain traversability prediction in unstructured environments. We show that our method is the state-of-the-art (SOTA) traversability mapping method on complex terrain datasets. Our method outperforms previous SOTA methods by 4.17% to 30.48% in terms of mAcc and reduces the MSE by 13.8% to 71.4%.
2. We have combined TTM with planning and control algorithms and evaluated their performance in real-world settings on an excavator in various challenging construction scenes, as shown in Figure 1. We show that our TTM-based planning algorithm can safely guide an excavator in unstructured environments and observe 49% improvement in terms of planning success rate.
3. We present the Complex Worksite Terrain (CWT) dataset, which consists of 30 minutes of video and 669 RGB images in unstructured environments with seven different classes based on terrain types, traversable regions, and obstacles. We will release the CWT dataset for any future works on perception in unstructured and hazardous environments.

We highlight the benefits of TTM in terms of first autonomous excavator that can navigate through complex, unstructured environments. We will release the implementation, terrain map outputs, and evaluation code that can reproduce the performance. The code and dataset link is shared in the supplemental material.

## 2. Related Work

### 2.1. Terrain Traversability Recognition

The concept of traversability, also referred to as "drivability", "navigability", etc. [30], has been discussed for decades. There are many viewpoints on the problems and challenges associated with traversability, and investigations into such topics have had different evaluation methods and goals. Many works focus on getting correct predictions of the terrain [5, 10, 13, 15, 16, 22, 26, 38, 46, 54] by some notion of ground truth based on human-labeled annotation, similar to the metrics of 2D and 3D semantic segmentation. Most of the methods mentioned above are based on visual features of the terrain, which sometimes lack the properties that enable real-world navigation due to recognition failure.

On the other hand, some works focus on obtaining traversability maps that result in the best navigation outcomes. There are plenty of works [2, 3, 9, 27, 31, 57] on classifying different terrains based on either material categories or navigability properties and demonstrate their mapping results through navigation outcomes.

However, those methods deal with structured roads or roads with clear path boundaries in unstructured environments. In more complex environments, pointclouds obtained from LiDAR are used to extract geometric attributes of the surface, including slope, height variation, roughness, obstacles, etc., as proposed in [1, 4, 6, 14, 49, 59]. [39] uses both pointcloud and RGB images to classify terrains with safe, risky, and obstacle labels in the 2D image plane for better performance. [37] presents a pipeline from perception to motion control and uses five different data sources for navigation, including range and intensity values from a 2D LiDAR, as well as edge information from an RGB-D camera. [19, 20] make some analysis of the terrain and create roadmaps for road safety. The works most similar to our proposed method are [9, 27, 44, 57], which focus on finding a better terrain representation for navigation in unstructured terrains.

### 2.2. Vision for Robotics

Many problems in robotics are considered downstream tasks of a computer vision problem, including matching and tracking for localization [28, 41], perception for planning and navigation [27, 57], etc. Accurate perception and good scene understanding are required for robotic applications so that the robot can interact with its surroundings.

Computer vision can solve robotic problems in a variety of industrial usages, including mining [42], excavation [56], agriculture [34], construction [29], etc. In addition, many practical concerns should be considered, including hardware issues, adaptability to new environments, robustness for corner cases, energy efficiency, and fast run-time for deploying an online system.

### 2.3. Datasets for Unstructured Environments

Most recent developments in perception tasks like object detection and semantic segmentation focus on urban driving scene datasets like KITTI [12], Waymo [45], etc., which achieve high accuracy in terms of average precision. On the other hand, unstructured scenes like the natural environment, construction sites, and complicated traffic scenarios are less explored, for two primary reasons. First, there are fewer datasets with unstructured environments; second, perception and autonomous navigation in unstructured off-road environments are challenging due to unpredictability and diverse terrain types.

Recent efforts in off-road perception and navigation include RUGD [50] and RELLIS-3D [17], which are semantic segmentation datasets collected from a robot navigating in off-road and natural environments. These datasets contain scenes like trails, forests, creeks, etc. [36] is a construction dataset containing annotation of heavy-duty vehicles for detection, tracking, and activity classifications.

## 3. Terrain Traversability Mapping

In this section, we present an efficient 2D-3D hybrid method for terrain traversability mapping (TTM) to extract terrain features and generate a traversability map as the robot navigates through an unknown environment. TTM takes a 3D pointcloud stream from the LiDAR, an RGB camera stream from the RGB camera, and the corresponding poses of the excavator extracted from the GPS-RTK module. The output of our method is a global map consisting of terrain information, including semantic information, geometric information, and a final traversability score.

### 3.1. Perception for Outdoor Excavators

The road conditions in structured environments such as highways are usually navigation-friendly, so the core problem during navigation in structured environments is avoiding obstacles rather than determining which part of the surface is easier and safer to navigate. In contrast, excavators are usually operated in unstructured and dangerous environments consisting of rock piles, cliffs, deep pits, steep hills, etc. Such an environment lacks any lane markings, and the arrangement of obstacles tends to be non-uniform. In addition, due to tasks like digging and dumping, the working conditions for excavators are constantly changing. Landfalls and cave-ins occur, potentially causing the excavator

to tip over and injure the operator. Therefore, it is crucial to identify different terrains and predict safe regions for navigation.

The definition of traversability is, according to [30], the capability of a ground vehicle to reside over a terrain region under an admissible state wherein it is capable of entering given its current state. In order to solve navigation challenges for excavators as well as other working vehicles in unstructured terrain, we formulate the problem of obtaining an accurate traversability map representation as follows:

**Problem Definition:** Given sensor inputs  $S_1, S_2, \dots, S_h$  from  $h$  different sources, over a time span  $T$ , the goal is to obtain a 2D grid map  $T \in [0, 1]^{H \times W}$  with resolution  $r$ , where  $T$  corresponds to some region  $R$  of shape  $(Hr, Wr)$ . The maximum value 1 corresponds to a non-traversable region, while the minimum value 0 corresponds to the most traversable region.

**Metrics for Traversability Map:** We need to consider the following measurements in excavator applications:

- **Accuracy:** Similar to [9, 39, 44], we use an ROC curve to measure the accuracy of the traversability prediction. In addition, the map output should fit the terrain closely, so we also use MSE (mean squared error) as a fitness measurement.
- **Performance:** [27, 57] use navigation outcome to measure their terrain traversability mapping algorithms, which include travel time, success rate, etc.
- **Energy constraints and run-time:** Due to the limitations of hardware and power supply on the excavator, energy efficiency and run-time should also be measured in a terrain traversability mapping method.

**Our Solution – TTM:** The map is represented as an elevation grid map and is updated based on incoming pointclouds and RGB images. Internally, each grid cell in the map stores the average height value of the latest  $p$  points within this cell, as well as overall information about those points like update time, slope, step height, and their semantic information. A traversability score is calculated for each grid cell. In Figure 2, we present an overview of our approach. Our code is based on the open-source gridmap library [11].

### 3.2. Segmentation and Mapping to Pointcloud

We use 2D semantic segmentation on unstructured terrains. Given an input RGB image  $I \in \mathbb{R}^{3 \times H \times W}$ , the goal is to generate a mask  $P \in \{0, 1, \dots, N - 1\}^{H \times W}$ , where  $N$  is the number of classes. We use Fast-SCNN [32] after leveraging accuracy and efficiency, as shown in Table 2.

After we get the segmentation prediction  $P$ , we use a timestamp to locate the corresponding pointcloud  $C$  and use camera calibration matrices to find the correspondence of each point to the segmentation results and save the terrain label in the gridmap cell.

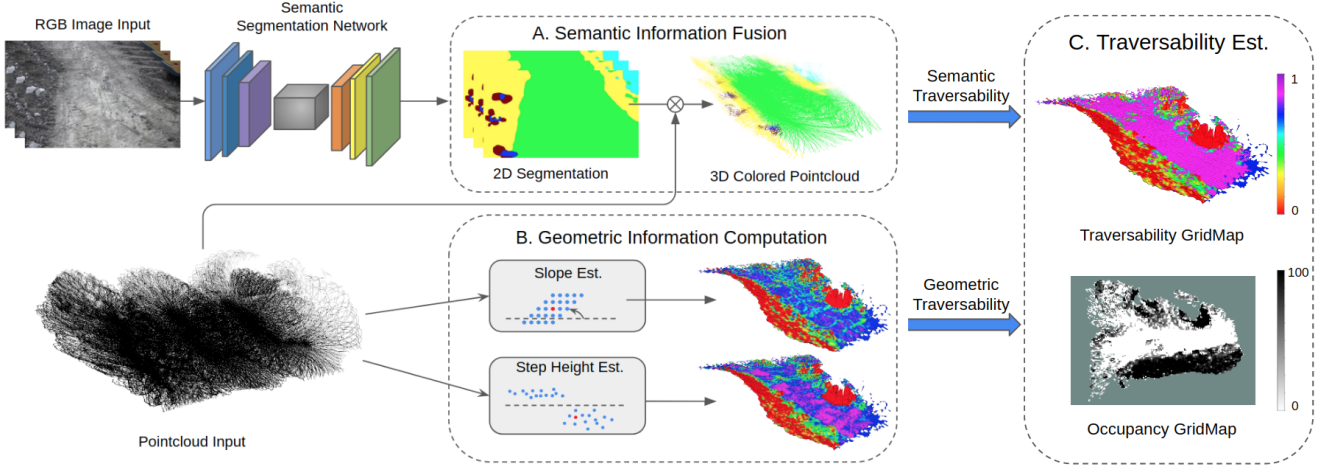


Figure 2. **Overview of our method (TTM):** Our method takes RGB images and pointclouds as inputs to infer traversability. We extract semantic information using segmentation and associate terrain labels with pointclouds, as shown in A (top). We extract geometric information using slope and step height estimation, as shown in B (bottom). Finally, we produce a traversability gridmap based on semantic and geometric information and convert it to a 2D occupancy map for path planning, as shown in C (right).

### 3.3. Geometric Information Computation

In this section, we present details of slope and step height estimation and highlight how machine specifications are considered to calculate geometric traversability score.

**Slope Estimation:** Each grid cell  $g$  is abstracted to a single point  $p = \{x, y, z\}$ , where  $x, y$  is the center of the cell in the global coordinate frame and  $z$  is the height value of the grid. The slope  $s$  in arbitrary grid cell  $g$  is computed by the angle between the surface normal and the  $z$ -axis<sup>1</sup> of the global coordinate frame:

$$s = \arccos(n^z), n^z \in [0, 1]$$

where  $n^z$  is the component of normal  $\vec{n}$  on the  $z$ -axis.

We use Principal Component Analysis (PCA) to calculate the normal direction of a grid cell. The covariance matrix  $C_{cov}$  of the nearest neighbors of the query grid cell is calculated as follows:

$$C_{cov} = \frac{1}{k} \sum_{i=1}^k (p_i - \bar{p}) \cdot (p_i - \bar{p})^T, C_{cov} \cdot \vec{v}_j = \lambda_j \cdot \vec{v}_j,$$

$$j \in \{0, 1, 2\}, \lambda_i < \lambda_j \text{ if } i < j,$$

where  $k$  is the number of neighbors considered in the neighborhood of  $g$ ,  $p_i = \{x, y, z\}$  is the position of the neighbor grid in the global coordinate frame,  $\bar{p}$  is the 3D centroid of the neighbors,  $\lambda_j$  is the  $j$ -th eigenvalue of the covariance matrix, and  $\vec{v}_j$  is the  $j$ -th eigenvector. The surface normal  $\vec{n}$  of grid  $g$  is the eigenvector  $\vec{v}_0$  with the smallest absolute value of eigenvalue  $\lambda_0$ .

The purpose of the slope estimation is to get the shape of the terrain and avoid navigating on a steep surface. For excavator applications, the width between the tracks or wheels

is a good indicator of the navigation stability on rough terrain. Usually, when the area of a rough region is less than half the width between the excavator's tracks, the excavator can navigate through it without any trouble. Specifically in our excavator setup, the width of our excavator track is  $0.6 \text{ m}$ , so we chose the grid resolution  $d_{res} = 0.2 \text{ m}$  and search the nearest eight neighbors, which covers the necessary area.

**Step Height Estimation:** The step height  $h$  is computed as the largest height difference between the center point  $p$  of the grid and its  $k'$  nearest neighbors:

$$h = \max(\text{abs}(p^z - p_i^z)), i \in [1, k']$$

Since slope is a description of variation in the terrain in a relatively small region, we choose to use a neighbor search parameter  $k' = 7 * 7 > k$  that spans  $1.4 \text{ m}$  to measure height change in a larger scope. For excavator applications, the step height calculation guarantees that the track does not traverse areas with extreme height differences.

**Geometric Traversability Estimation:** Based on information about slope and step height of the terrain, we can calculate a geometric traversability score  $T_{geo}$ . According to the physical constraints of the robot, we create some critical values  $s_{cri}, s_{safe}, h_{cri}, h_{safe}$ , as the thresholds for safety and danger detection. The purpose of those threshold values is to avoid danger when the surface condition exceeds the limits of the robot and to avoid more calculations when the surface is very flat. The formula for geometric traversability  $T_{geo}$  for each grid is:

$$T_{geo} = \begin{cases} 0 & s > s_{cri} \text{ or } h > h_{cri} \\ 1 & s < s_{safe} \text{ and } h < h_{safe} \\ \max(1 - (\alpha_1 \frac{s}{s_{cri}} + \alpha_2 \frac{h}{h_{cri}}), 0) & \text{otherwise} \end{cases}$$

where the weights  $\alpha_1$  and  $\alpha_2$  sum up to 1.

<sup>1</sup>Up direction in the real world

The step height estimation is complementary to slope estimation; it provides a global perspective, whereas slope is local terrain information. Combining these two specifications can help us remove noise in the map, such as bumps caused by dust, and ensure the robustness of the  $T_{geo}$ .

### 3.4. Traversability with Geometric and Semantic Fusion

In this section, we describe our algorithm for geometric-semantic fusion. From the semantic and geometric information, we use a continuous traversability score  $T \in [0, 1]$  to measure how easily the surface can be navigated. This is especially relevant to off-road scenarios because we prefer flat regions over bumpy roads to save energy. Moreover, when an excavator is navigating on a construction site, being able to correctly identify different regions is critical to avoid hazardous situations like flipping over.

The overall traversability score  $T$  is calculated based on semantic terrain classes  $C_{sem}$  and geometric traversability  $T_{geo}$  on each grid:

$$T = \begin{cases} 0 & C_{sem} = \{\text{rock, excavator, obstacle, water}\} \\ 1 & C_{sem} = \{\text{flat}\} \text{ and } T_{geo} > 0 \\ T_{geo} & \text{otherwise} \end{cases},$$

This method is simple yet more effective than other comparably complicated fusion methods [44, 57], as demonstrated in Section 6 and Section 7.

## 4. TTM-based Planning and Navigation

We deploy our approach TTM on an excavator as part of the Autonomous Excavator System [56]. The AES system has a pipeline of perception, planning, and navigation modules. We integrate and evaluate our method through planning results and real-world navigation performance by using our mapping output, as shown in Figure 3. Note that previous AES systems mainly focus on digging tasks, while our method focuses on providing accurate mapping estimation for navigation in unstructured environments.

**Post-processing after TTM:** We have a post-processing step on the traversability map before planning. We remove some non-traversable regions that satisfy all of the following criteria:

- The region has a traversability value less than some occupied threshold  $t_{occ}$ .
- The spans of the region along the x-axis and the y-axis satisfy both: 1) less than half the distance between two tracks of the excavator  $d_{track}$  and 2) an average height less than the height  $h_{cab}$ , which is the distance from the bottom of the cabin to the ground.

This post-processing step is mostly to accommodate existing planners, since they do not work well and fail to plan a feasible trajectory with too many scattered, noisy regions.

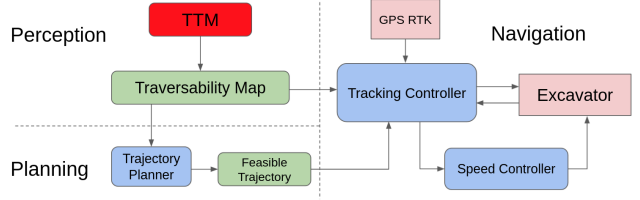


Figure 3. **TTM-based planning for autonomous excavation:** We show the components of AES as blue blocks and highlight our method TTM using a red block. We use green blocks to represent the TTM-based trajectory computation module.

**TTM-Based Planning:** We use Hybrid A\* [24] to calculate a trajectory based on the traversability map output from TTM after post-processing step. Hybrid A\* is a global path planner based on a 2D occupancy gridmap as an input for path planning. The planner will generate a path and send the trajectory motion controllers, which guide the excavator to follow this trajectory.

We briefly explain other components in AES framework:

- **Tracking Controller:** This module can adjust the steering of the robot for path following.
- **Speed Controller:** This module can adjust the speed of the robot.

More results based on TTM-integrated planner and its benefits are given in Section 7.

## 5. Complex Worksite Terrain (CWT) Dataset

In this section, we present the Complex Worksite Terrain (CWT) dataset, which is collected at a construction site while an excavator is navigating through the work area. The hardware has the same setup as described in Section 7.1. We collect three videos (30 minutes in total) under different circumstances and annotate 669 images of size  $1920 \times 1080$  according to terrain semantics. We only highlight the ontology and differences between CWT and other off-road datasets [17, 50], and provide details of the collection, class distribution, and analysis in the supplemental material.

The CWT dataset is annotated with seven labels based on terrain features and navigability, as shown in Table 1. The annotation is decided based on the opinion of a team of

Types	Descriptions	Navigability	Distribution
Flat Region	Flat surfaces that most vehicles like cars can traverse.	Easy	41.76%
Bumpy Region	Bumpy surfaces that most vehicles can not traverse except working vehicles like excavators.	Medium	42.59%
Rock Pile	Very common on work-site; Need to be avoided most of the time.	Forbidden	6.51%
Water	Water might be trapped in deep trench after raining; Need to be avoided.	Forbidden	3.66%
Mixtures of Water and Dirt	Shallow water with mostly visible soil or dirt; Can be traversed.	Medium	4.90%
Excavator & Vehicles	Common vehicles that appear on work-site, like excavators.	Forbidden	0.35%
Obstacles	Uncommon objects that need to be avoided, like steel bar, sign block, etc.	Forbidden	0.23%

Table 1. **CWT Ontology:** Classification of Terrain Features

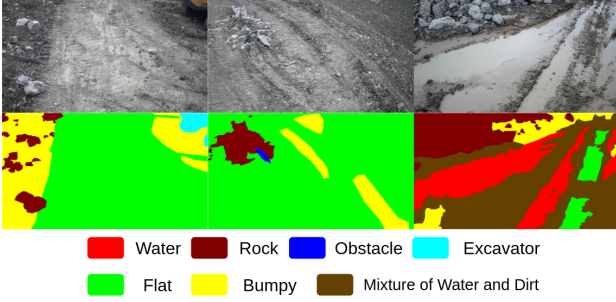


Figure 4. **Complex Worksite Terrain (CWT) dataset:** We show a few samples from our CWT dataset (**top**) and corresponding annotations (**bottom**). All images are collected in unstructured environments with various terrain types.

excavator operators. In most cases, when flat surfaces are detected, they are preferable to other surfaces.

While the CWT dataset and other datasets like RUGD [50] and RELLIS-3D [17] are collected in unstructured, outdoor environments, the CWT has several distinctions. As shown in Figure 4, the CWT dataset mostly consists of uneven terrain with unfavorable road conditions and covers many situations that might be encountered on a work site, including rock-piles, pits, stagnant water after rain, etc.

In addition, the CWT dataset focuses entirely on roads and terrains, and the annotation is based on terrain semantics instead of fine-grained semantics on every possible classes. Such annotation scheme is designed for the benefit of other downstream tasks, including planning and navigation for robots of any sizes, and excavation activities on hazardous terrains.

Overall, CWT presents many new challenges to the vision community to improve perception outcomes in hazardous environment, while considering efficiency in terms of autonomous robotics applications. We show the performances of several SOTA semantic segmentation methods on the CWT and RELLIS-3D dataset in Section 6. We will release this dataset.

## 6. Experiments and Evaluations

In Section 6.1, we show evaluation results for the semantic segmentation task on our CWT dataset and RELLIS-3D [17]. In Section 6.2, we evaluate TTM algorithm on RELLIS-3D and show the benefits of our method compared to other SOTA mapping methods.

### 6.1. Perception Evaluation on the CWT Dataset

We show some evaluations using several SOTA segmentation methods on CWT dataset and RELLIS-3D dataset in Table 2. The CWT poses more challenges as a terrain dataset compared to RELLIS-3D. In particular, we also highlight the number of parameters and GFLOPS as a measurement since energy efficiency is an important factor for

Methods	Params ↓	Dataset	mIoU ↑	mAcc ↑	Img Size	GFLOPs ↓
CGNet [52]	<b>0.494 M</b>	CWT	53.41	67.59	1920 x 1080	27.62
		RELLIS	65.9	79.25	1920 x 1200	30.67
Fast SCNN [32]	1.45 M	CWT	54.77	68.75	1920 x 1080	<b>7.45</b>
		RELLIS	69.27	80.99	1920 x 1200	<b>8.03</b>
Fast FCN [51]	68.7 M	CWT	41.68	51.85	1920 x 1080	1031.51
		RELLIS	68.24	79.21	1920 x 1200	1145.6
BiSeNetV2 [55]	14.77 M	CWT	54.37	67.05	1920 x 1080	97.51
		RELLIS	65.33	75.06	1920 x 1200	108.38
SETR* [58]	109.67 M	CWT	19.91	30.61	1920 x 1080	–
		RELLIS	65.53	76.57	1920 x 1200	–
		–	–	–	1024 x 512	337.46†
DPT* [35]	309.17 M	CWT	29.02	47.65	1920 x 1080	–
		RELLIS	55.38	66.23	1920 x 1200	–
		–	–	–	1024 x 512	424.87†
Segformer [53]	3.72 M	CWT	50.6	64.29	1920 x 1080	50.55†
		RELLIS	68.62	83.4	1920 x 1200	–

Table 2. **Perception Accuracy on the CWT and RELLIS-3D [17] Dataset:** We list several SOTA semantic segmentation methods and train the model with 240K iterations. The CWT dataset has lower accuracy compared to RELLIS dataset. \* marks methods that do not converge well after 240K additional iterations. † marks the GFLOPs as an approximation and a lower bound.

robotic applications. The method and evaluation for segmentation is based on MMSeg [7].

### 6.2. Terrain Traversability Map Evaluation

We evaluate our method and compare it with several SOTA traversability mapping methods on the RELLIS-3D dataset. We use the ground truth semantic labels from RELLIS-3D on 3D pointcloud and convert the labels to either 0 or 1 to indicate traversability on a gridmap. During evaluation, we assume that the traversability map is based on the Clearpath Warthog, the same robot that collected the RELLIS-3D dataset: traversable regions like grass, dirt, concrete, and asphalt are set to 0, while puddles, bushes, and obstacles are set to 1. Even though our method outputs a continuous value between 0 and 1, we want to simplify the conversion between labels and traversability scores to avoid any biases.

#### 6.2.1 Comparisons

Since many methods do not have publicly available codes, we implement their methods based on the papers, which can only run on an offline dataset but not in the real world. We compare our method with the following methods:

**Dahlkamp et al. [9]** use a Mixture of Gaussian Model to make a binary prediction on RGB images for traversable regions and make an inverse perspective transform to the world coordinates.

**Sock et al. [44]** use a Linear Support Vector Machine for a 2-classes prediction and some mapping between terrain slope and a traversability score between 0 and 1. The final map is obtained through Bayes Fusion of terrain classification and slope information.

Methods	Modality	Goal	Trav / Non-Trav Acc $\uparrow$	mAcc $\uparrow$	aAcc $\uparrow$	AUC $\uparrow$	MSE $\downarrow$
KPConv* [47]	LiDAR	3D segmentation	33.33 / 79.24	56.28	67.65	-	0.253
SalsaNet* [8]	LiDAR	3D segmentation	94.82 / 57.75	76.28	67.11	-	0.370
Chilian et al. [6]	LiDAR	Mapping & Navigation	66.19 / 88.29	77.24	82.17	0.790	0.155
Dahlkamp et al. [9]	RGB Camera	Navigation	4.41 / 99.91	52.16	54.42	0.751	0.123
Zhao et al. [57]	LiDAR + Stereo Camera	Mapping & Navigation	9.31 / 99.85	54.58	56.67	0.528	0.128
Sock et al. [44]	LiDAR + RGB Camera	Mapping & Navigation	1.93 / 99.93	50.93	53.21	0.590	0.156
TTM (ours)	LiDAR + RGB Camera	Mapping & Navigation	71.77 / 91.05	<b>81.41</b>	<b>85.70</b>	<b>0.803</b>	<b>0.106</b>

Table 3. **SOTA comparisons:** We list several methods and show our benefits on an offline RELLIS [17] dataset.

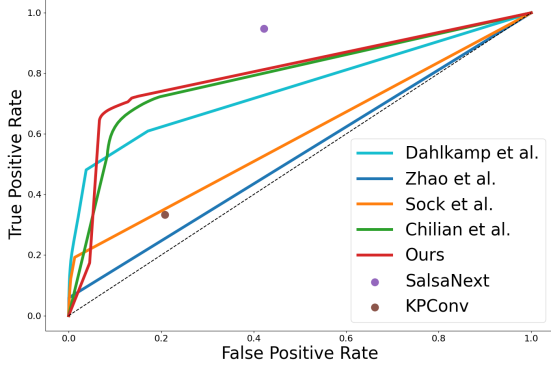


Figure 5. **ROC plot:** We plot ROCs on several SOTA mapping/segmentation methods. In particular, LiDAR-based segmentation methods [8, 47] are trained on the pointcloud labels, so they have the advantage of prior knowledge on the ground truth. In the real world, annotated 3D pointcloud data would not been easily available for applications. We use a point in the ROC plot to represent those methods, as there is not a threshold to adjust.

**Zhao et al. [57]** use a multi-class segmentation method based on RGB images and make projections onto a gridmap for planning and navigation. In particular, Maturana et al. [27] use a distance transformation and update new observations with Bayes’s rule.

**Geometric-based methods [6, 59]** only use geometric information from the pointcloud for navigation tasks.

**3D semantic segmentation [8, 47] methods** are useful for classifying terrains and predicting traversability. We obtain their inference results from the official repository of RELLIS-3D [17].

### 6.2.2 Evaluation Metrics and Results

We evaluate the traversability map based on offline data with four different metrics. In general, our method has better performance in terms of accuracy and MSE. Note that in the first three metrics, all traversability values are converted to either 0 or 1 for methods that have a continuous output. The metrics are described as follows:

**Mean Accuracy:** The average accuracy of traversable and non-traversable region.

**All Accuracy:** Accuracy over all grids.

**ROC (Receiver Operation Curve):** Previous methods [9, 44] make binary predictions over each grid, so ROC is a common indicator of the performance through true positive and false positive rates, as shown in Figure 5.

**MSE (Mean Squared Error):** To describe how well the prediction fits the ground truth, we also calculate the average distance between the prediction and the ground truth over all grids in Table 3.

## 7. Performance in the Real World

In this section, we show some visual results based on real-world data and show planning and navigation performance based on TTM in the real world. Since there is no code available for other methods with online implementation, we use geometric components of our method and adjust accordingly. This method is referred to as the geometric-only method [6] in the rest of this section.

### 7.1. Hardware setup

We use an XCMG XE490D excavator to perform our experiments. The excavator is equipped with a Livox-Mid100 LiDAR, a HIK web camera with FOV of 56.8 degrees with a pitch angle of 30.3 degrees to detect the environment, and a Huace real-time kinematic (RTK) positioning device to provide the location. We run our code on a laptop with an Intel Core i7-10875H CPU, 16 GB RAM, and 6GB GeForce RTX 2060 on the excavator.

XCMG XE490D excavator has a maximum climbing angle of 35 degrees, and a typical recommended climbing angles for any vehicle as a safe climbing angle, which is 10 degrees. Therefore, we set  $s_{cri} = 35 \text{ deg}$  and  $s_{safe} = 10 \text{ deg}$ . In addition, we obtain an approximation of the maximum height allowed by  $s_{cri}$  and  $s_{safe}$ , after expanding three times the resolution  $d_{res}$  along the surface to get:

$$h_{cri} = 3 \tan(s_{cri}) \times d_{res} = 0.35 \text{ m}$$

$$h_{safe} = 3 \tan(s_{safe}) \times d_{res} = 0.10 \text{ m}$$

### 7.2. Visual Results and Analysis

In this section, we evaluate our method in the real world with visual results. In Figure 6, we show some typical scenarios excavators encounter to illustrate the advantages of

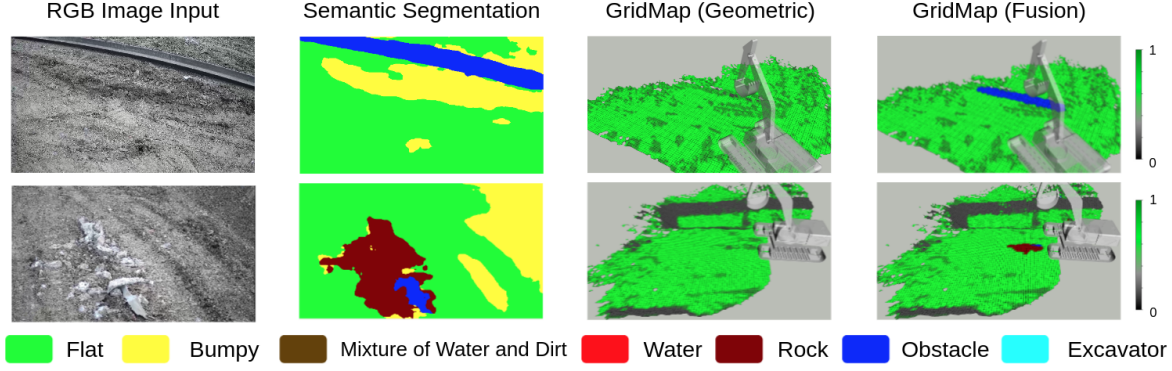


Figure 6. **Visual results of TTM:** In the traversability map, the higher the traversability score, the easier it is for robots to navigate the corresponding terrain. More visual results are available in the supplemental material.

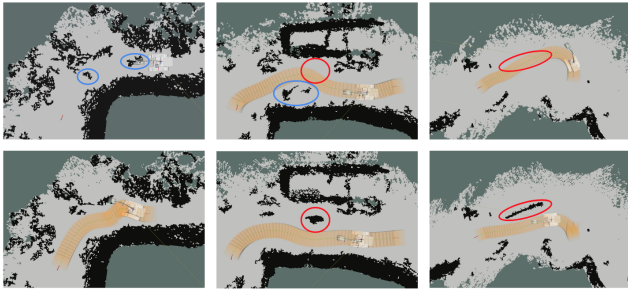


Figure 7. **Planner output comparisons between geometric-only scheme [6] (top) and TTM (bottom):** We show planned trajectories with the Hybrid A\* [24] planner. The planning is based on a global traversability map. We highlight some obstacles that are not observed by geometric method (red), as well as some traversable regions that are falsely observed by geometric method (blue).

geometric and semantic fusion. In those cases, the steel bar and stone were not captured by geometric calculation, while with semantic information, those obstacles can be detected.

### 7.3. Planning Based on a Traversability Map

Based on the resulting occupancy gridmaps from the proposed TTM and geometric-only method [6], we randomly choose start and goal positions on an unoccupied grid with over 90 trials. The success rates of finding a valid path without collision for our TTM and the other method are 82.6% and 33.3%, respectively. We show some comparisons on planning results in Figure 7. In particular, we use an occupied threshold  $t_{occ}$  of 0.6. The height of the cabin  $h_{cab}$  is 0.5 m, and the distance between two tracks  $d_{track}$  is 2.75 m for map post-processing and planner configuration.

### 7.4. Run-time Analysis

Our method consists of the following major parts, which contribute to the overall runtime of the system:

- **Segmentation** generates a pixel-wise semantic classification on each image in the RGB input stream.
- **Projection** casts the 2D segmentation result onto the 3D pointcloud and assigns each point a semantic label

Run-time (ms)	Max	Min	Mean
Segmentation	100.2	53.5	75.4
Projection	54.0	35.0	42.3
$T_{geo}$ Calculation	38.0	9.0	22.1

Table 4. **Runtimes of different modules.** Our method can be run in real-time and update the traversability map at a rate of 10 Hz.

through the calibration matrix.

- **Geometric traversability calculation** estimates and updates slope and step height based on pointcloud data in gridmap representation.

In Table 4, we give details of the run-time of each component in the system. The final fusion step is under 2 ms and does not contribute to the overall runtime of the method. Our method can update the traversability map at a rate of 10 Hz. Please refer to the video for more visual results of excavator navigation.

## 8. Conclusions, Limitations, and Future Work

In this paper, we present Terrain Traversability Mapping (TTM), a novel terrain traversability mapping strategy based on 2D semantic information and 3D geometric information, and show application benefits on difficult excavator navigation tasks in the real world. We prepare the CWT dataset with difficult real-world scenes in unstructured construction sites for perception in the wild.

Our work has some limitations. First, due to safety issues, we are not able to extensively test our planning algorithm in all type of scenarios. Second, we have tested our performance on existing planners, which are not able to exploit the full benefits of traversability. For example, sometimes the excavator would have been able to run over small obstacles with the space between two tracks. As part of our future work, we would like to design improved planners and utilize the specifications of the excavator like a human operator. We would also like to evaluate the performance in different types of outdoor terrains.

## References

- [1] Juhana Ahtiainen, Todor Stoyanov, and Jari Saarinen. Normal distributions transform traversability maps: Lidar-only approach for traversability mapping in outdoor environments. *Journal of Field Robotics*, 34(3):600–621, 2017. 2
- [2] Mohammed Abdessamad Bekhti and Yuichi Kobayashi. Regressed terrain traversability cost for autonomous navigation based on image textures. *Applied Sciences*, 10(4), 2020. 2
- [3] Mauro Bellone, Giulio Reina, Luca Caltagirone, and Mattias Wahde. Learning traversability from point clouds in challenging scenarios. *IEEE Transactions on Intelligent Transportation Systems*, 19(1):296–305, 2018. 2
- [4] Tim Braun, Henning Bitsch, and Karsten Berns. Visual terrain traversability estimation using a combined slope/elevation model. In Andreas R. Dengel, Karsten Berns, Thomas M. Breuel, Frank Bomarius, and Thomas R. Roth-Berghofer, editors, *KI 2008: Advances in Artificial Intelligence*, pages 177–184, Berlin, Heidelberg, 2008. Springer Berlin Heidelberg. 2
- [5] R. Omar Chavez-Garcia, Jérôme Guzzi, Luca M. Gambardella, and Alessandro Giusti. Learning ground traversability from simulations. *IEEE Robotics and Automation Letters*, 3(3):1695–1702, 2018. 2
- [6] Annett Chilian and Heiko Hirschmüller. Stereo camera based navigation of mobile robots on rough terrain. In *2009 IEEE/RSJ International Conference on Intelligent Robots and Systems*, pages 4571–4576, 2009. 1, 2, 7, 8
- [7] MMSegmentation Contributors. MMSegmentation: Openmmlab semantic segmentation toolbox and benchmark. <https://github.com/open-mmlab/mms Segmentation>, 2020. 6
- [8] Tiago Cortinhal, George Tzelepis, and Eren Erdal Aksoy. Salsanext: Fast, uncertainty-aware semantic segmentation of lidar point clouds for autonomous driving, 2020. 7
- [9] Hendrik Dahlkamp, Adrian Kaehler, David Stavens, Sebastian Thrun, and Gary R. Bradski. Self-supervised monocular road detection in desert terrain. In *Robotics: Science and Systems*, 2006. 1, 2, 3, 6, 7
- [10] Fucheng Deng, Xiaorui Zhu, and Chao He. Vision-based real-time traversable region detection for mobile robot in the outdoors. *Sensors*, 17(9), 2017. 2
- [11] Péter Fankhauser and Marco Hutter. A universal grid map library: Implementation and use case for rough terrain navigation. In *Robot Operating System (ROS)*, pages 99–120. Springer, 2016. 3
- [12] A Geiger, P Lenz, C Stiller, and R Urtasun. Vision meets robotics: The kitti dataset. *The International Journal of Robotics Research*, 32(11):1231–1237, 2013. 3
- [13] Tianrui Guan, Divya Kothandaraman, Rohan Chandra, and Dinesh Manocha. Ganav: Group-wise attention network for classifying navigable regions in unstructured outdoor environments, 2021. 1, 2
- [14] Robert A Hewitt, Alex Ellery, and Anton de Ruiter. Training a terrain traversability classifier for a planetary rover through simulation. *International Journal of Advanced Robotic Systems*, 14(5):1729881417735401, 2017. 2
- [15] Noriaki Hirose, Amir Sadeghian, Marynel Vázquez, Patrick Goebel, and Silvio Savarese. Gonet: A semi-supervised deep learning approach for traversability estimation. In *2018 IEEE/RSJ International Conference on Intelligent Robots and Systems (IROS)*, pages 3044–3051, 2018. 2
- [16] Christopher J. Holder and Toby P. Breckon. Learning to drive: Using visual odometry to bootstrap deep learning for off-road path prediction. In *2018 IEEE Intelligent Vehicles Symposium (IV)*, pages 2104–2110, 2018. 2
- [17] Peng Jiang, Philip R. Osteen, Maggie Wigness, and Srikanth Saripalli. Rellis-3d dataset: Data, benchmarks and analysis. *2021 IEEE International Conference on Robotics and Automation (ICRA)*, pages 1110–1116, 2021. 3, 5, 6, 7
- [18] Gregory Kahn, Pieter Abbeel, and Sergey Levine. Badgr: An autonomous self-supervised learning-based navigation system. *IEEE Robotics and Automation Letters*, 6(2):1312–1319, 2021. 1
- [19] Muhammad Khan, Karsten Berns, and Abubakr Muhammad. Vehicle specific robust traversability indices using roadmaps on 3d pointclouds. *International Journal of Intelligent Robotics and Applications*, 4:1–17, 12 2020. 2
- [20] Muhammad Mudassir Khan, Haider Ali, Karsten Berns, and Abubakr Muhammad. Road traversability analysis using network properties of roadmaps. In *2016 IEEE/RSJ International Conference on Intelligent Robots and Systems (IROS)*, pages 2960–2965, 2016. 2
- [21] Sung-Keun Kim and J. Russell. Framework for an intelligent earthwork system: Part i. system architecture. *Automation in Construction*, 12:1–13, 2003. 1
- [22] Nathaniel Kingry, Myungjin Jung, Evan Derse, and Ran Dai. Vision-based terrain classification and solar irradiance mapping for solar-powered robotics. In *2018 IEEE/RSJ International Conference on Intelligent Robots and Systems (IROS)*, pages 5834–5840, 2018. 2
- [23] Ashish Kumar, Zipeng Fu, Deepak Pathak, and Jitendra Malik. Rma: Rapid motor adaptation for legged robots, 2021. 1
- [24] Karl Kurzer. Path planning in unstructured environments : A real-time hybrid a\* implementation for fast and deterministic path generation for the kth research concept vehicle. Master’s thesis, 2016. 5, 8
- [25] Roberto Manduchi, A. Castano, Ashit Talukder, and L. Matthies. Obstacle detection and terrain classification for autonomous off-road navigation. *Autonomous Robots*, 18:81–102, 01 2005. 1
- [26] Sango Matsuzaki, Kimitoshi Yamazaki, Yoshitaka Hara, and Takashi Tsubouchi. Traversable region estimation for mobile robots in an outdoor image. *J. Intell. Robotic Syst.*, 92(3-4):453–463, 2018. 2
- [27] Daniel Maturana, Po-Wei Chou, Masashi Uenoyama, and Sebastian Scherer. Real-time semantic mapping for autonomous off-road navigation. In Marco Hutter and Roland Siegwart, editors, *Field and Service Robotics*, pages 335–350, Cham, 2018. Springer International Publishing. 1, 2, 3, 7
- [28] Raul Mur-Artal, J. Montiel, and Juan Tardos. Orb-slam: a versatile and accurate monocular slam system. *IEEE Transactions on Robotics*, 31:1147 – 1163, 10 2015. 2

- [29] Nipun D. Nath and A. Behzadan. Deep convolutional networks for construction object detection under different visual conditions. In *Frontiers in Built Environment*, 2020. 3
- [30] Panagiotis Papadakis. Terrain traversability analysis methods for unmanned ground vehicles: A survey. *Engineering Applications of Artificial Intelligence*, 26(4):1373–1385, 2013. 2, 3
- [31] David Paz, Hengyuan Zhang, Qinru Li, Hao Xiang, and Henrik I. Christensen. Probabilistic semantic mapping for urban autonomous driving applications. In *2020 IEEE/RSJ International Conference on Intelligent Robots and Systems (IROS)*, pages 2059–2064, 2020. 2
- [32] Rudra P. K. Poudel, Stephan Liwicki, and R. Cipolla. Fast-scn: Fast semantic segmentation network. In *BMVC*, 2019. 3, 6
- [33] Michael J. Procopio, Jane Mulligan, and Greg Grudic. Learning terrain segmentation with classifier ensembles for autonomous robot navigation in unstructured environments. *Journal of Field Robotics*, 26(2):145–175, 2009. 1, 2
- [34] Redmond R Shamshiri, Cornelia Weltzien, Ibrahim A Hameed, Ian J Yule, Tony E Grift, Siva K Balasundram, Lenka Pitonakova, Desa Ahmad, and Girish Chowdhary. Research and development in agricultural robotics: A perspective of digital farming. 2018. 3
- [35] Rene Ranftl, Alexey Bochkovskiy, and Vladlen Koltun. Vision transformers for dense prediction. In *ICCV*, 2021. 6
- [36] Dominic Roberts and Mani Golparvar-Fard. End-to-end vision-based detection, tracking and activity analysis of earthmoving equipment filmed at ground level. *Automation in Construction*, 2019. 3
- [37] Ryan D. Rosenfeld, Mark G. Restrepo, William H. Gerard, Walter E. Bruce, Atiena A. Branch, Gregory C. Lewin, and Nicola Bezzo. Unsupervised surface classification to enhance the control performance of a ugv. In *2018 Systems and Information Engineering Design Symposium (SIEDS)*, pages 225–230, 2018. 2
- [38] Brandon Rothrock, Ryan Kennedy, Christopher T. Cunningham, Jeremie Papon, Matthew Heverly, and Masahiro Ono. Spoc: Deep learning-based terrain classification for mars rover missions. 2016. 2
- [39] Fabian Schilling, Xi Chen, John Folkesson, and Patric Jensfelt. Geometric and visual terrain classification for autonomous mobile navigation. In *2017 IEEE/RSJ International Conference on Intelligent Robots and Systems (IROS)*, pages 2678–2684, 2017. 2, 3
- [40] Jongwon Seo, Seungsoo Lee, Jeonghwan Kim, and Sung-Keun Kim. Task planner design for an automated excavation system. *Automation in Construction*, 20(7):954–966, 2011. 1
- [41] Tixiao Shan and Brendan Englott. Lego-loam: Lightweight and ground-optimized lidar odometry and mapping on variable terrain. In *IEEE/RSJ International Conference on Intelligent Robots and Systems (IROS)*, pages 4758–4765. IEEE, 2018. 2
- [42] H. Shariati, Anuar Yeraliyev, B. Terai, S. Tafazoli, and Mahdi Ramezani. Towards autonomous mining via intelligent excavators. In *CVPR Workshops*, 2019. 3
- [43] Anukriti Singh, Kartikeya Singh, and P. B. Sujit. Offroad-transeg: Semi-supervised segmentation using transformers on offroad environments, 2021. 1
- [44] Juil Sock, Jun Kim, Jihong Min, and Kiho Kwak. Probabilistic traversability map generation using 3d-lidar and camera. In *2016 IEEE International Conference on Robotics and Automation (ICRA)*, pages 5631–5637, 2016. 1, 2, 3, 5, 6, 7
- [45] Pei Sun, Henrik Kretzschmar, Xerxes Dotiwalla, Aurelien Chouard, Vijaysai Patnaik, Paul Tsui, James Guo, Yin Zhou, Yuning Chai, Benjamin Caine, et al. Scalability in perception for autonomous driving: Waymo open dataset. In *Proceedings of the IEEE/CVF Conference on Computer Vision and Pattern Recognition*, pages 2446–2454, 2020. 3
- [46] Vivekanandan Suryamurthy, Vignesh Sushrutha Raghavan, Arturo Laurenzi, Nikos G. Tsagarakis, and Dimitrios Kanoulas. Terrain segmentation and roughness estimation using rgb data: Path planning application on the centauro robot. In *2019 IEEE-RAS 19th International Conference on Humanoid Robots (Humanoids)*, pages 1–8, 2019. 2
- [47] Hugues Thomas, Charles R. Qi, Jean-Emmanuel Deschaud, Beatriz Marcotegui, François Goulette, and Leonidas J. Guibas. Kpconv: Flexible and deformable convolution for point clouds. *Proceedings of the IEEE International Conference on Computer Vision*, 2019. 7
- [48] Kasi Viswanath, Kartikeya Singh, Peng Jiang, P.B. Sujit, and Srikanth Saripalli. Offseg: A semantic segmentation framework for off-road driving. In *2021 IEEE 17th International Conference on Automation Science and Engineering (CASE)*, pages 354–359, 2021. 1
- [49] Martin Wermelinger, Péter Fankhauser, Remo Diethelm, Philipp Krüsi, Roland Siegwart, and Marco Hutter. Navigation planning for legged robots in challenging terrain. In *2016 IEEE/RSJ International Conference on Intelligent Robots and Systems (IROS)*, pages 1184–1189, 2016. 2
- [50] Maggie Wigness, Sungmin Eum, John G Rogers, David Han, and Heesung Kwon. A rugd dataset for autonomous navigation and visual perception in unstructured outdoor environments. In *International Conference on Intelligent Robots and Systems (IROS)*, 2019. 3, 5, 6
- [51] Huikai Wu, Junge Zhang, Kaiqi Huang, Kongming Liang, and Yu Yizhou. Fastfcn: Rethinking dilated convolution in the backbone for semantic segmentation, 2019. 6
- [52] Tianyi Wu, Sheng Tang, Rui Zhang, and Yongdong Zhang. Cgnet: A light-weight context guided network for semantic segmentation. *IEEE Transactions on Image Processing*, 30:1169–1179, 2021. 6
- [53] Enze Xie, Wenhai Wang, Zhiding Yu, Anima Anandkumar, Jose M. Alvarez, and Ping Luo. Segformer: Simple and efficient design for semantic segmentation with transformers. In *Thirty-Fifth Conference on Neural Information Processing Systems*, 2021. 6
- [54] Jia Xue, Hang Zhang, K. Dana, and K. Nishino. Differential angular imaging for material recognition. *2017 IEEE Conference on Computer Vision and Pattern Recognition (CVPR)*, pages 6940–6949, 2017. 2
- [55] Changqian Yu, Changxin Gao, Jingbo Wang, Gang Yu, Chunhua Shen, and Nong Sang. Bisenet v2: Bilateral net-

- work with guided aggregation for real-time semantic segmentation. *International Journal of Computer Vision*, 129:1–18, 11 2021. [6](#)
- [56] Liangjun Zhang, Jinxin Zhao, Pinxin Long, Liyang Wang, Lingfeng Qian, Feixiang Lu, Xibin Song, and Dinesh Manocha. An autonomous excavator system for material loading tasks. *Science Robotics*, 6(55), 2021. [1](#), [3](#), [5](#)
  - [57] Yimo Zhao, Peilin Liu, Wuyang Xue, Ruihang Miao, Zheng Gong, and Rendong Ying. Semantic probabilistic traversable map generation for robot path planning. In *2019 IEEE International Conference on Robotics and Biomimetics (ROBIO)*, pages 2576–2582, 2019. [1](#), [2](#), [3](#), [5](#), [7](#)
  - [58] Sixiao Zheng, Jiachen Lu, Hengshuang Zhao, Xiatian Zhu, Zekun Luo, Yabiao Wang, Yanwei Fu, Jianfeng Feng, Tao Xiang, Philip H.S. Torr, and Li Zhang. Rethinking semantic segmentation from a sequence-to-sequence perspective with transformers. In *CVPR*, 2021. [6](#)
  - [59] Yan Zhou, Ying Huang, and Zhenhua Xiong. 3d traversability map generation for mobile robots based on point cloud. In *2021 IEEE/ASME International Conference on Advanced Intelligent Mechatronics (AIM)*, pages 836–841, 2021. [2](#), [7](#)